Contribution from the Departments of Chemistry, University of Denver, Denver, Colorado 80208, and University of Colorado at Denver, Denver, Colorado 80202

Metal–Nitroxyl Interactions. 26. Impact of an Additional Atom in the Metal–Nitroxyl Linkage on the Magnitude of Electron–Electron Spin–Spin Coupling Constants in Spin-Labeled Pyridine Adducts of Vanadyl and Copper(II) Bis(β-diketonates)

JYOTI K. MORE, KUNDALIKA M. MORE, GARETH R. EATON,* and SANDRA S. EATON

Received October 27, 1981

Electron–electron coupling constants, J, have been obtained from solution EPR spectra for a series of spin-labeled pyridines coordinated to vanadyl bis(trifluoroacetylacetonate), vanadyl bis(hexafluoroacetylacetonate), and copper bis(hexafluoroacetylacetonate). The value of J was larger for a ligand with a urea linkage between the pyridine ring and the nitroxyl ring than for a ligand with an amide linkage. The addition of a CH_2 group between the pyridine ring and the amide or urea linkage led to a decrease in the value of J. The impact of the additional CH_2 group was greater for the urea linkage than for the amide linkage and was greater for the 4-substituted pyridine ligands than for the 3-substituted pyridine ligands. The observed dependence of J on linkage is attributed to a π-interaction pathway in the urea ligands.

Introduction

Electron–nuclear hyperfine coupling constants are widely used to determine electron spin density distributions in paramagnetic species.[1] However, because of the line widths typically observed in EPR spectra and the multiplicity of lines in complex spectra, resolved hyperfine coupling can only be obtained for positions with relatively large spin density.[1] ENDOR spectra can be used to measure smaller electron–nuclear coupling constants but ENDOR spectra can only be obtained on systems in which the electron spin relaxation time is sufficiently long to permit saturation.[2] NMR of paramagnetic molecules can also be used to measure small electron–nuclear coupling constants, but it is limited to systems in which the electron spin relaxation time is sufficiently short that an averaged signal is observed for the two electron spin states on the NMR time scale.[3] Recent results from our laboratories have shown that electron–electron spin–spin coupling constants can provide information concerning spin delocalization that complements that which can be obtained by other methods.[4–9] Since the electron magnetic moment is much larger than nuclear magnetic moments, electron–electron coupling can be observed for much smaller spin densities than electron–nuclear coupling. Furthermore, electron–electron spin–spin coupling can be observed in the EPR spectra when the electron spin relaxation time is too short for ENDOR measurements and too long for paramagnetic NMR. We have used the changes in electron–electron coupling constants, J, to monitor changes in electron spin delocalization due to changes in metal ion,[4,5] changes in metal–nitroxyl linkages,[6–9] and changes in ligand conformation.[5–8]

In this paper we examine the effect on electron–electron spin–spin coupling when a CH_2 or NH group is used to lengthen the bonding pathway between a paramagnetic transition metal and a nitroxyl radical. We have analyzed the EPR spectra of a series of spin-labeled pyridines coordinated to vanadyl bis(hexafluoroacetylacetonate), $VO(hfac)_2$, vanadyl bis(trifluoroacetylacetonate), $VO(tfac)_2$, and copper bis(hexafluoroacetylacetonate), $Cu(hfac)_2$. We had previously reported results for ligands I and II.[5] We have now examined ligands III–VII, in which an additional CH_2, NH, or $(CH_2)_2$ group has been added between the pyridine and nitroxyl rings.

Experimental Section

Physical Measurements. Infrared spectra were obtained in halocarbon or Nujol mulls on a Perkin-Elmer 337 grating spectrometer. X-Band EPR spectra were obtained on a Varian E-9 spectrometer[10] with use of deoxygenated solutions. Solution concentrations were 1

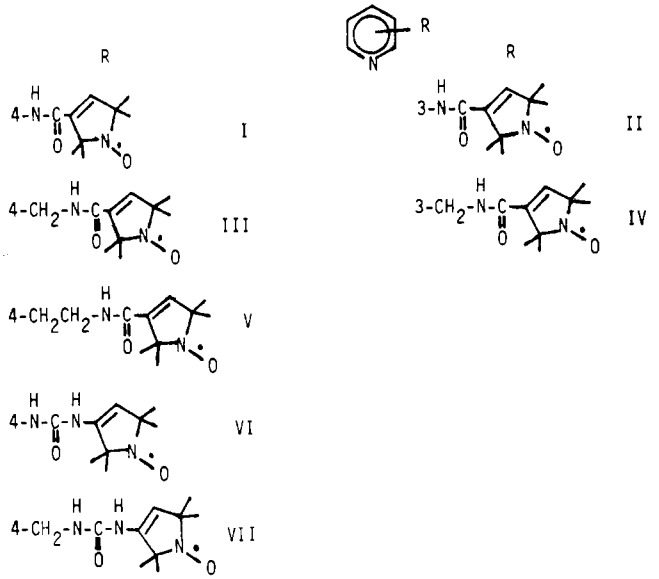

$\times 10^{-3}$ to 5×10^{-3} M. g values were measured relative to DPPH (2.0036). All coupling constants are given in gauss (1 G = 0.1 mT) to facilitate comparison with the field-swept experimental spectra. Elemental analyses were performed by Spang Microanalytical Laboratory.

Preparation of Compounds. All starting materials were commercially available and were used as received unless specified otherwise. The following compounds were prepared by literature methods: $Cu(hfac)_2$,[11] $VO(tfac)_2$,[12] and $VO(hfac)_2$.[13]

* To whom correspondence should be addressed at the University of Denver.

(1) Wertz, J. E.; Bolton, J. R. "Electron Spin Resonance: Elementary Theory and Practical Applications"; McGraw-Hill: New York, 1972; Chapters 5 and 6.
(2) Kevan, L.; Kispert, L. D. "Electron Spin Double Resonance Spectroscopy"; Wiley-Interscience: New York, 1976; Chapter 1.
(3) LaMar, G. N.; Horrocks, W. DeW.; Holm, R. H. "NMR of Paramagnetic Molecules: Principles and Applications"; Academic Press: New York, 1973; Chapters 1 and 3.
(4) More, K. M.; Eaton, S. S.; Eaton, G. R. *J. Am. Chem. Soc.* **1981**, *103*, 1087–1090.
(5) Sawant, B. M.; Shroyer, A. L. W.; Eaton, G. R.; Eaton, S. S. *Inorg. Chem.* **1982**, *21*, 1093–1101 and references therein.
(6) More, K. M.; Eaton, S. S.; Eaton, G. R. *Inorg. Chem.* **1981**, *20*, 2641–2647.
(7) Sawant, B. M.; Braden, G. A.; Smith, R. E.; Eaton, G. R.; Eaton, S. S. *Inorg. Chem.* **1981**, *20*, 3349–3354.
(8) More, K. M.; Sawant, B. M.; Eaton, G. R.; Eaton, S. S. *Inorg. Chem.* **1981**, *20*, 3354–3362.
(9) More, K. M.; Eaton, G. R.; Eaton, S. S. *Can. J. Chem.*, in press.
(10) More, K. M.; Eaton, G. R.; Eaton, S. S. *Inorg. Chem.* **1979**, *18*, 2492–2496.
(11) Funck, L. L.; Ortolano, T. R. *Inorg. Chem.* **1968**, *7*, 567–573.
(12) Rowe, R. A.; Jones, M. M. *Inorg. Synth.* **1957**, *5*, 113–116.
(13) Su, C.; Reed, J. W.; Gould, E. S. *Inorg. Chem.* **1973**, *12*, 337–343. Drago, R. S.; Kuechler, T. C.; Kroeger, M. *Ibid.* **1979**, *18*, 2337–2342.

0020-1669/82/1321-2455$01.25/0

4-[(((2,2,5,5-Tetramethyl-1-oxypyrrolin-3-yl)carbonyl)amino)methyl]pyridine (III). The acid chloride of 3-carboxy-2,2,5,5-tetramethylpyrrolin-3-yl-1-oxy[14] (1.1 g) was treated with the dry THF (75 mL), pyridine (2 mL) and 4-(aminomethyl)pyridine (0.45 g). The reaction mixture was refluxed overnight, and the solvent was removed under vacuum. The residue was dissolved in $CHCl_3$ (75 mL). The $CHCl_3$ solution was washed several times with 0.1 N NaOH (total volume ca. 200 mL), washed once with water, and dried over anhydrous Na_2SO_4. The solvent was removed under vacuum. The residue was dissolved in $CHCl_3$ and put on a silica gel column. Impurities were eluted with $CHCl_3$. The product eluted with 2% methanol in $CHCl_3$ as a slow-moving yellow band and was recrystallized from benzene/hexane: yield 40%; mp 110 °C. IR: ν_{CO} 1660, ν_{NH} 3300 cm^{-1}. EPR (CH_2Cl_2): g = 2.0059, A_N = 14.6 G. Anal. Calcd for $C_{15}H_{20}N_3O_2$: C, 65.67; H, 7.35; N, 15.32. Found: C, 65.50; H, 7.25; N, 15.33.

3-[(((2,2,5,5-Tetramethyl-1-oxypyrrolin-3-yl)carbonyl)amino)methyl]pyridine (IV). The amide was prepared from the acid chloride of 3-carboxy-2,2,5,5-tetramethylpyrrolin-3-yl-1-oxy[14] and 3-(aminomethyl)pyridine as reported for III: yield 50%; mp 124 °C. IR: ν_{CO} 1670, ν_{NH} 3250 cm^{-1}. EPR (CH_2Cl_2): g = 2.0059, A_N = 14.6 G. Anal. Calcd for $C_{15}H_{20}N_3O_2$: C, 65.67; H, 7.35; N, 15.32. Found: C, 65.55; H, 7.35; N, 15.39.

4-[(((2,2,5,5-Tetramethyl-1-oxypyrrolin-3-yl)carbonyl)amino)ethyl]pyridine (V). The amide was prepared from the acid chloride of 3-carboxy-2,2,5,5-tetramethylpyrrolin-3-yl-1-oxy and 4-(aminoethyl)pyridine as reported for III: yield 60%; mp 95 °C. IR: ν_{CO} 1660, ν_{NH} 3200 cm^{-1}. EPR (CH_2Cl_2): g = 2.0059, A_N = 14.6 G. Anal. Calcd for $C_{16}H_{22}N_3O_2$: C, 66.64; H, 7.69; N, 14.57. Found: C, 66.75; H, 7.58; N, 14.58.

4-[(((2,2,5,5-Tetramethyl-1-oxypyrrolin-3-yl)amino)carbonyl)amino]pyridine (VI). 3-Isocyanato-2,2,5,5-tetramethylpyrrolin-3-yl-1-oxy[15] (1.83 g) was added to a solution of 4-aminopyridine (0.94 g) in THF (75 mL). The reaction mixture was refluxed overnight, and then the solvent was removed in vacuum. The residue was dissolved in $CHCl_3$ and chromatographed on a silica gel column. Impurities were eluted with $CHCl_3$. The product eluted with 2% methanol in $CHCl_3$ as a slow-moving yellow band and was recrystallized from CH_2Cl_2/hexane: yield 40%; mp 167 °C. IR: ν_{CO} 1710, ν_{NH} 3300 cm^{-1}. EPR (CH_2Cl_2): g = 2.0060, A_N = 14.6 G. Anal. Calcd for $C_{14}H_{19}N_4O_2$: C, 61 07; H, 6.96; N, 20.35. Found: C, 60.99; H, 6.89; N, 20.27.

4-[((((2,2,5,5-Tetramethyl-1-oxypyrrolin-3-yl)amino)carbonyl)amino)methyl]pyridine (VII). The urea was prepared by reaction of 3-isocyanato-2,2,5,5-tetramethylpyrrolin-3-yl-1-oxy[15] with 4-(aminomethyl)pyridine as reported for VI: yield 50%; mp 146 °C. IR: ν_{CO} 1700, ν_{NH} 3375 cm^{-1}. EPR (CH_2Cl_2): g = 2.0060, A_N = 14.6 G. Anal. Calcd for $C_{15}H_{21}N_4O_2$: C, 62.26; H, 7.32; N, 19.36. Found: C, 62.19; H, 7.22; N, 19.41.

Computer Simulations

The computer program CUNO[5,16] was used to simulate the EPR spectra.

In the absence of nuclear spins the Hamiltonian for two coupled electrons would be

$$\mathcal{H} = \beta\vec{H}(g_1\vec{S}_1 + g_2\vec{S}_2) + hJ\vec{S}_1\cdot\vec{S}_2 \quad (1)$$

Expansion in terms of $\hat{S}_+$, $\hat{S}_-$, and $\hat{S}_Z$ and inclusion of nuclear spins gives eq 2, the Hamiltonian used in the program, where

$$\mathcal{H} = g_1\beta H\hat{S}_{1Z} + g_2\beta H\hat{S}_{2Z} + hJ\hat{S}_{1Z}\hat{S}_{2Z} + (hJ/2)(\hat{S}_{1+}\hat{S}_{2-} + \hat{S}_{1-}\hat{S}_{2+}) + hA_M\hat{S}_{1Z}\hat{I}_{1Z} + hA_N\hat{S}_{1Z}\hat{I}_{2Z} + hA_{N'}\hat{S}_{2Z}\hat{I}_{3Z} + (hA_M/2)(\hat{S}_{1+}\hat{I}_{1-} + \hat{S}_{1-}\hat{I}_{1+}) - g_M\beta_N H\hat{I}_{1Z} - g_N\beta_N H\hat{I}_{2Z} - g_{N'}\beta_N H\hat{I}_{3Z} \quad (2)$$

g_1 and g_2 are the g values of the metal and nitroxyl electrons, $\vec{S}_1$ and $\vec{S}_2$ refer to the metal and nitroxyl electron spins, respectively, J is the electron–electron coupling constant in hertz; I_1, I_2, and I_3 refer to the metal nuclear spin, the nuclear spin of the coordinated nitrogens, and the nuclear spin of the nitroxyl nitrogen, respectively, A_M is the metal electron–metal nuclear coupling constant in hertz, A_N is the coupling constant in hertz between the metal electron and the nuclear spins of the coordinated nitrogens, $A_{N'}$ is the coupling constant in hertz between the nitroxyl electron and the nuclear spin of the nitroxyl nitrogen, and all other symbols are defined as in ref 16. The first seven terms in the Hamiltonian were treated exactly, and the last four were treated as a perturbation to second order for the transition energies and to first order for the transition probabilities.

Table I. Electron–Electron Coupling Constants, J[a]

L	VO(tfac)$_2$·L	VO(hfac)$_2$·L	Cu(hfac)$_2$·L
I	400[b] (22)	375[b] (22)	160[b] (22)
	475		175[b] (−25)
II	94[b] (22)	95[b] (22)	60[b] (22)
	85[b] (−40)		180[b] (−25)
III	30 (22)	21 (22)	2 (22)
	24 (−60)		16 (−60)
	29		
IV	8[c] (22)	~5[c] (22)	~16[c] (22)
	23 (−60)		27 (−40)
V	<4 (22)	<4 (22)	<2 (22)
	<2 (−60)		<3 (−60)
VI	485 (22)	550 (22)	227 (22)
	565		300 (−40)
VII	2.5 (22)	4 (22)	<2 (22)
	7.4 (−60)		<2 (22)

[a] Values are given in gauss for spectra taken at X band. The temperature at which each value was obtained is given in parentheses (°C). For ligands I and II spectra were taken in $CHCl_3$-, CH_2Cl_2-, or C_2HCl_3/toluene solution. For ligands III–VII all spectra were taken in CH_2Cl_2. [b] Value taken from ref 5. [c] Broad lines make the value of J uncertain.

So that visual comparison with the field-swept experimental spectra could be facilitated, the values of J, A_M, A_N, and $A_{N'}$ are discussed in units of gauss with the conversion between hertz and gauss given by eq 3–5. The conversion factor for A_N is the same as for A_M. Only the absolute value of J can be determined from these experiments.

$$J\,(\mathrm{G}) = [J\,(\mathrm{Hz})]\frac{h}{2\beta}\left(\frac{1}{g_1} + \frac{1}{g_2}\right) \quad (3)$$

$$A_M\,(\mathrm{G}) = [A_M\,(\mathrm{Hz})]\frac{h}{g_1\beta} \quad (4)$$

$$A_{N'}\,(\mathrm{G}) = [A_{N'}\,(\mathrm{Hz})]\frac{h}{g_2\beta} \quad (5)$$

The electron–electron coupling results in AB patterns in the EPR spectra. The lines in the spectra are referred to as metal or nitroxyl depending on the nature of the transitions as $J \to 0$. When J is small relative to the g-value difference between the metal and nitroxyl electrons, each of the metal and nitroxyl lines is split into a doublet. As J becomes larger, the intensity of the outer lines of the AB pattern goes to zero and the positions of the inner metal and inner nitroxyl lines become equal.

The EPR parameters for VO(tfac)$_2$·py (g = 1.968 ± 0.001, A_V = 107.0 ± 0.5 G), VO(hfac)$_2$·py (g = 1.968 ± 0.001, A_V = 108.0 ± 0.5 G), and Cu(hfac)$_2$·py (g = 2.149 ± 0.001, A_{Cu} = 52.0 ± 1.0 G) were used as starting parameters in the simulations of the spectra of the analogous complexes with paramagnetic ligands. Best fit to the spectra in all cases required changes of 1.0 G or less in A_M and 0.002 or less in the g value. The nitroxyl parameters were g = 2.0059 ± 0.0002 and A_N = 14.3–15.0 G, depending on solvent and temperature. The values of J obtained from the simulations

(14) Rozantsev, E. G. "Free Nitroxyl Radicals"; translated by B. J. Hazzard; Plenum Press: New York, 1970; p 209.
(15) DuBois, D. L.; Eaton, G. R.; Eaton, S. S. *J. Am. Chem. Soc.* **1978**, *100*, 2686–2689.
(16) Eaton, S. S.; DuBois, D. L.; Eaton, G. R. *J. Magn. Reson.* **1978**, *32*, 251–263.

Table II. Parameters Used in Simulations of EPR Spectra

figure	component[a]	J, G	g_M	g_{NO}	A_M, G	A_{NO}, G	assignt	line width parameters[b] A	B	C
1A	$VO(tfac)_2$·VII (85%)	4.5	1.970	2.0059	106.5	14.8	V	c		
							NO(i)[d]	3.5	−0.2	0.0
							NO(o)[d]	3.5	0.0	0.0
	VII (15%)			2.0060		14.7		2.2	−0.1	0.0
1B	$VO(tfac)_2$·VII (88%)	6.7	1.970	2.0059	c	14.8	V	c		
							NO(i)[d]	3.2	−0.2	0.0
							NO(o)[d]	3.0	0.0	0.0
	VII (12%)			2.0060		14.7		1.7	0.0	0.0
2	$VO(hfac)_2$·VI (90%)	550	1.969	2.0059	108.0	14.5	V(o)[e]	25.8	0.45	0.27
							V(i)[e]	12.8	1.50	0.75
							NO(i)[e]	12.4	0.36	−0.23
							NO(o)[e]	22.7	−1.39	0.70
	$VO(hfac)_2$ (10%)		1.969		109.5			16.6	0.62	0.74
	VI (7%)			2.0058		14.5		2.0	0.0	0.0
3	$Cu(hfac)_2$·VI (78%)	227	2.1548	2.0059	52.0	14.5	Cu(o)[e]	36.3	10.1	3.1
							Cu(i)[e]	30.6	11.0	2.0
							NO(i)[e]	13	0	0
							NO(o)[e]	16	0	0
	$Cu(hfac)_2$ (15%)		2.139		70			30.5	5.0	0.0
	VI (13%)			2.0060		14.5		2.0	0.0	0.0
	dimer (7%)		2.141		54.0			32.0	7.5	0.0

[a] Percentages are based on initial concentrations of metal complex. [b] A, B, and C are the coefficients in the equation line width = $A + Bm_I + Cm_I^2$ where m_I is the metal or nitroxyl nitrogen nuclear spin. Inner and outer lines of the AB patterns are denoted by (i) and (o), respectively. [c] Incomplete motional averaging causes substantial uncertainty in the parameters for the metal lines. [d] m_I is the nuclear spin of the nitroxyl nitrogen. [e] m_I is the nuclear spin of the metal.

are given in Table I. The values of the parameters used to obtain the simulations shown in Figures 1–3 are given in Table II. These values are typical of the ones used in all of the simulations.

Results and Discussion

Solution Equilibria. Pyridine derivatives coordinate to $VO(tfac)_2$ and $VO(hfac)_2$ to give six-coordinate adducts. Our previous results indicate that these complexes have the geometry VIII in which the pyridine nitrogen is cis to the V=O

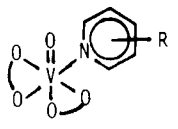

VIII

bond.[5] When a nitroxyl oxygen binds to $VO(tfac)_2$ or $VO(hfac)_2$, there is strong spin coupling between the vanadyl and nitroxyl unpaired electrons and there is no EPR signal for the nitroxyl or vanadyl electrons at room temperature.[17] Thus, the presence of nitroxyl oxygen bonded species in the equilibrium mixture does not cause difficulties in interpreting the EPR spectra. With ligands I–VII there is also some formation of dimeric species in which the pyridine nitrogen coordinates to one vanadyl bis(β-diketonate) and the nitroxyl oxygen coordinates to a second vanadyl bis(β-diketonate). The coupling between the nitroxyl unpaired electron and the vanadyl unpaired electron reduces the three-spin system to a one-spin system. The vanadyl coordinated to the pyridine end of the ligand gives the same eight-line spectrum as observed for $VO(tfac)_2$·py or $VO(hfac)_2$·py, which have slightly smaller values of A_V than in the free vanadyl complexes. In solutions containing approximately equimolar vanadyl bis(β-diketonate) and ligand, complex VIII is the predominant species and dimer formation has little impact on the EPR spectra. However, when excess metal complex is added, there is a substantial increase in dimer formation. Since traces of water in the solvent result in competing equilibria, no attempt was made to measure the equilibrium constants.

The coordination equilibria involving $Cu(hfac)_2$ and spin-labeled pyridines have been examined in detail.[18,19] The predominant species in solutions containing a 1:1 $Cu(hfac)_2$:ligand ratio is the 5-coordinate N-bonded pyridine adduct.[18,19]

EPR Spectra of the Vanadyl Complexes. When the electron–electron coupling constant, J, is smaller than the EPR line widths, it does not cause resolved splitting of the lines. The EPR spectrum then consists of a superposition of the typical eight-line pattern for the vanadyl unpaired electron and the three-line pattern for the nitroxyl unpaired electron. Such spectra were obtained for $VO(tfac)_2$·V and $VO(hfac)_2$·V. The value of J for $VO(tfac)_2$·VII is also small at room temperature but increases as the temperature is decreased. Since the nitroxyl line widths are narrower than the vanadyl line widths, small coupling constants are more readily resolved for the nitroxyl lines than for the vanadyl lines. Figure 1 shows the EPR spectra of the nitroxyl lines for $VO(tfac)_2$·VII in CH_2Cl_2 solution at 0 and −42 °C. The small sharp three-line pattern is due to the spin-labeled ligand VII, which is not coordinated to $VO(tfac)_2$. At 0 °C the value of J is so small that resolved splitting is not observed, but the computer simulations indicated that a J of 4.5 G was needed to fit the observed line shape. However, at −42 °C the value of J is sufficiently large (6.7 G) that the nitroxyl signal is split into a doublet of triplets.

When J is greater than about 8 G at room temperature, splitting can be observed in both the vanadyl lines and the nitroxyl lines. For a J of about 20–30 G as observed for the vanadyl complexes of ligands III and IV, the vanadyl lines are a doublet of octets and the nitroxyl lines are a doublet of triplets. The spectra are similar to those shown in Figure 1 of ref 5.

The EPR spectrum of $VO(hfac)_2$·VI is shown in Figure 2. The computer-simulated spectrum was obtained with J = 550 G. When J is this large, there is substantial overlap of the vanadyl and nitroxyl regions of the spectrum and the outer

(17) Sawant, B. M.; Eaton, G. R.; Eaton, S. S. *J. Magn. Reson.* **1981**, *45*, 162–169.

(18) Boymel, P. M.; Eaton, G. R.; Eaton, S. S. *Inorg. Chem.* **1980**, *19*, 727–735.

(19) Boymel, P. M.; Braden, G. A.; Eaton, G. R.; Eaton, S. S. *Inorg. Chem.* **1980**, *19*, 735–739.

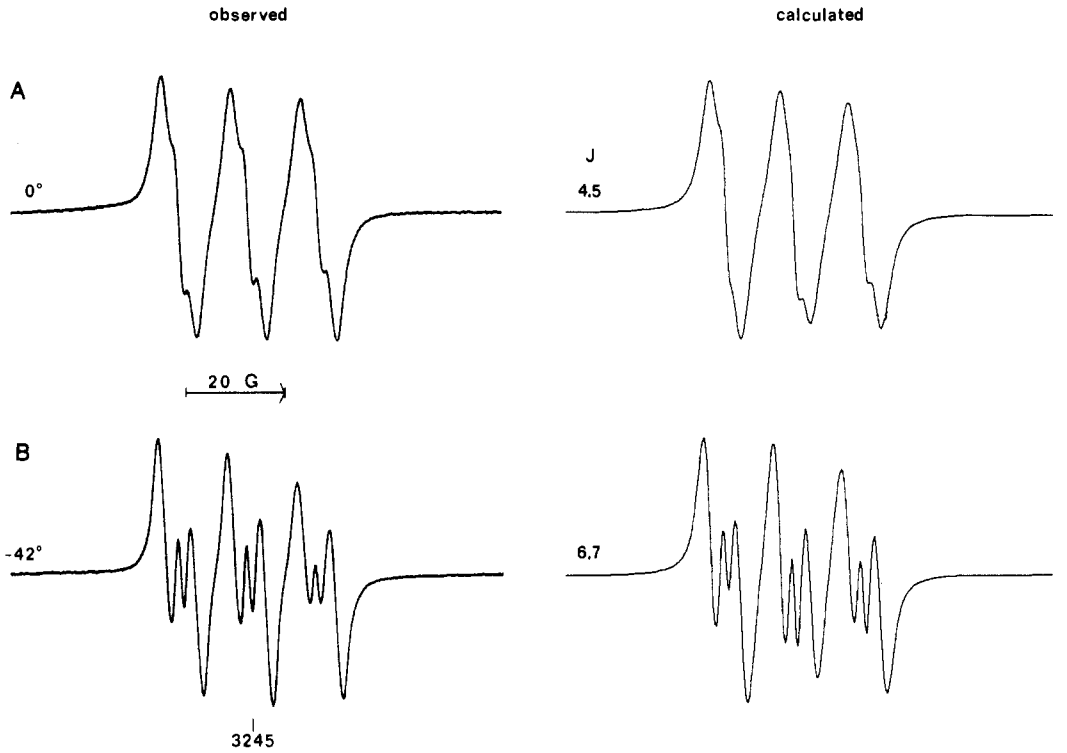

Figure 1. X-Band (9.108 GHz) EPR of the nitroxyl region of the spectra of $VO(tfac)_2$·VII in CH_2Cl_2 and computer simulations: (A) 0 °C, 100-G scan obtained with 2-mW power and 0.25-G modulation amplitude; (B) −42 °C, 100-G scan obtained with 5-mW power and 0.32-G modulation amplitude. Values of J are in gauss.

lines of the AB patterns are significantly less intense than the inner lines. The assignments of the lines in the spectrum are shown below the computer-simulated spectrum. The assignments are based on the assumption that A_V is negative,[20] but the analysis of the spectra does not depend on this assumption. The sharp three-line pattern centered at 3245 G is due to free ligand VI (7%). Free $VO(hfac)_2$ (10%) contributes eight lines to the spectrum. Each vanadyl line couples to each nitroxyl signal to give an AB pattern, which is labeled with the vanadyl nuclear spin state. Since the nitrogen hyperfine splitting of the nitroxyl lines is well resolved in the experimental spectrum, it is included in the assignment scheme. The splitting of the metal lines by the nitroxyl nitrogen spin is not resolved in the experimental spectrum, and so it is not included in the assignment scheme, although it was included in the simulations. The patterns centered at about 2570 and 4000 G are due to the vanadyl outer lines. The nitroxyl outer lines are centered at 2800 and 3750 G. The low-field set of nitroxyl outer lines was partially obscured by the $m_I = -^7/_2$ line of $VO(hfac)_2$, and the high-field set of nitroxyl outer lines was almost completely obscured by the $m_I = +^7/_2$ line of $VO(hfac)_2$. Since the vanadyl −0.5 line overlaps the nitroxyl triplet, there is very little intensity in the outer lines for these three AB patterns and there are both metal and nitroxyl outer lines in both the low-field and the high-field regions for these AB patterns.

The EPR spectra of $VO(tfac)_2$·VI show two isomers with J = 485 and 565 G. These are assigned to the isomers IX and X as previously discussed for $VO(tfac)_2$·I.[5] Similarly for $VO(tfac)_2$·III, two isomers were observed at −60 °C.

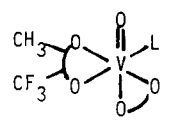

IX

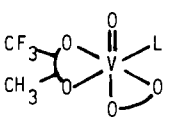

X

The values of J for the $VO(tfac)_2$ and $VO(hfac)_2$ adducts with ligands III–VII in CH_2Cl_2 solution are summarized in Table I. Values of J for the adducts of ligands I and II[5] are included for comparison. Results from spectra obtained at low temperature are also included. The g and A anisotropy of the vanadyl electron results in severe line broadening of the vanadyl signals at temperatures below about 0 °C. Thus, the temperature dependence of J for the spin-labeled vanadyl complexes was based on the nitroxyl lines as a function of temperature. For ligands I and VI all the lines in the spectra of the vanadyl complexes are broad at low temperature, and so studies were limited to room-temperature spectra.

The EPR spectra of the $VO(tfac)_2$ adducts of ligands III, IV, and VII were more strongly temperature dependent than was previously observed for other spin-labeled pyridine adducts of $VO(tfac)_2$.[5] In each case the value of J increased and the line widths decreased as the temperature was decreased. The line width changes as a function of temperature were greater than those for other complexes, which indicates that the narrowing was due to intramolecular processes rather than a decrease in collision broadening. Each of these ligands has a CH_2 group between the pyridine ring and the amide or urea linkage to the nitroxyl ring. At room temperature there may be considerable conformational mobility around the CH_2 carbon, which could result in an uncertainty in J and a broadening of the lines.[5,7-9] This motion would be expected to decrease at lower temperature, consistent with the observed narrowing of the lines. The substantially larger values of J at low temperature than those at high temperature suggest that the preferred conformations of the ligand permit greater spin delocalization than the higher energy conformations.

EPR Spectra of the Copper Complexes. The interpretation of the EPR spectra of $Cu(hfac)_2$ adducts of spin-labeled pyridines has been reported.[18,19] The EPR spectra of the adducts with ligands III–VII have been analyzed analogously. The values of J in CH_2Cl_2 are summarized in Table I.

The EPR spectrum of $Cu(hfac)_2$·VI at room temperature is shown in Figure 3. The simulated spectrum was obtained

(20) Wilson, R.; Kivelson, D. *J. Chem. Phys.* **1966**, *44*, 154–168.

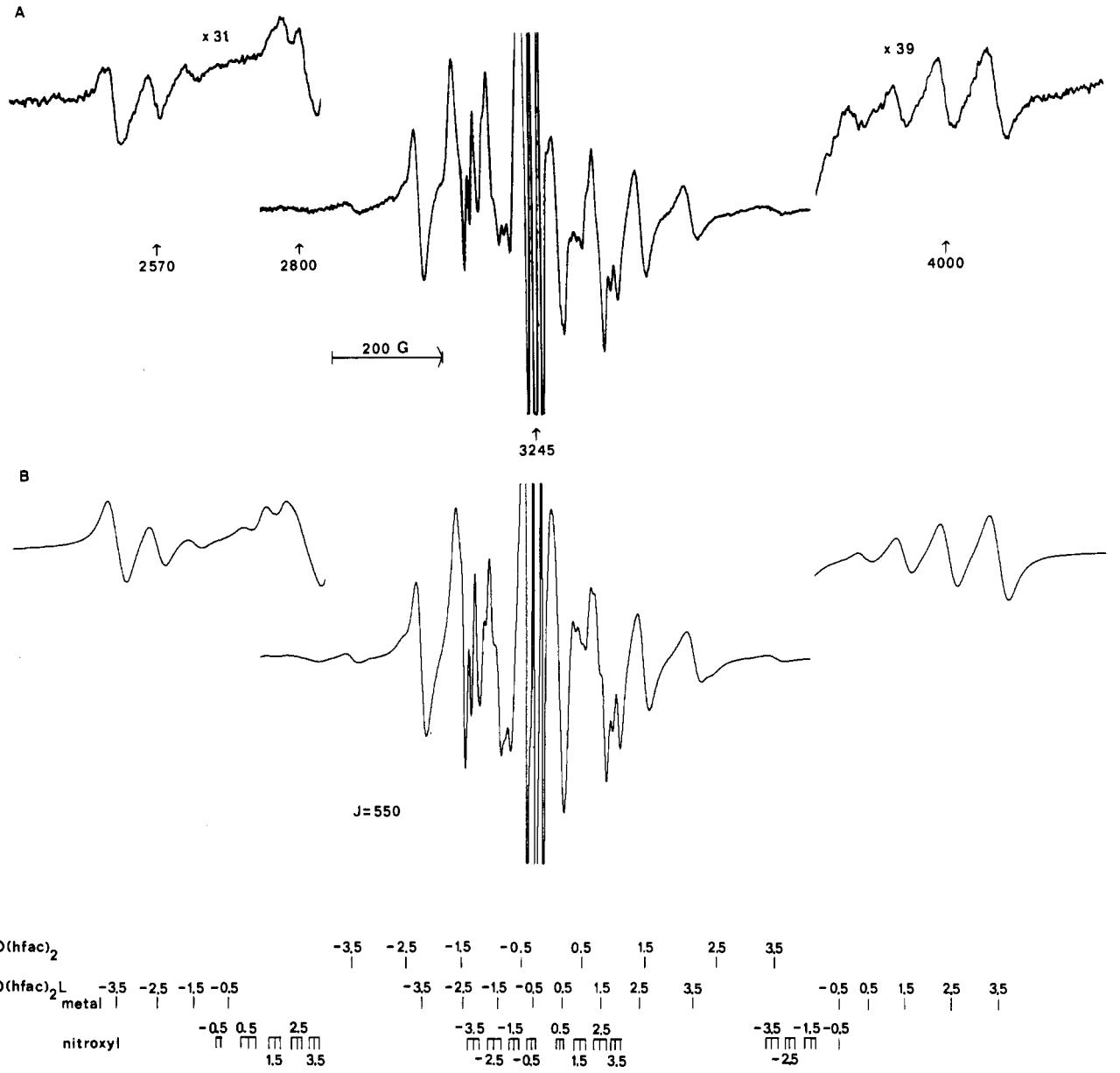

Figure 2. X-Band (9.108 GHz) EPR spectra of $VO(hfac)_2$·VI in CH_2Cl_2 solution at room temperature. (A) 1000-G scan of the inner lines of the AB pattern obtained with 40-mW power and 0.63 G modulation amplitude. The inserts show the outer lines of the AB pattern, which were obtained by time averaging 10 scans with the product of modulation amplitude, gain, and square root of power 31 times (low field) or 39 times (high field) greater than for the center lines of the spectrum. (B) Computer-simulated spectra calculated with J = 550 G. The assignments for the lines are given below the spectrum; see text for details.

with J = 227 G. The assignments of the lines marked on the simulated spectrum are given in the figure caption. On the basis of the total copper concentration, the relative contributions are as follows: $Cu(hfac)_2$·VI, 78%; $Cu(hfac)_2$, 15%; free VI, 13%; $Cu(hfac)_2$·VI·$Cu(hfac)_2$ dimer, 7%.

The values of J for the copper complexes are temperature dependent. We have noted previously that the range of geometries available to the five-coordinate adducts results in substantial temperature dependence of J.[5] It is difficult to separate the effects of the changes at the metal center from the effects of mobility around the CH_2 group. However, it is apparent that comparisons of the values of J should be made at low temperature, wherever solubilities and line widths permit.

Effect of an Additional NH Group on the Value of J. Comparison of the values of J for the 4-substituted ligands I and VI indicates that the additional NH group (urea vs. amide linkage) causes a small increase in the value of J for both the vanadyl and the copper adducts. Our prior results on ester, amide, and Schiff base linkages indicated that the values of J correlated with the double-bond character of the C–N bond or C–O bond in the pyridine–nitroxyl linkage.[5]

NMR studies of N,N′-disubstituted ureas have found that the barrier to rotation about the C–N bond is about half that observed for amides.[21-24] ^{13}C and ^{15}N chemical shifts indicate that there is less delocalization of the nitrogen lone pair in ureas than in amides.[25] Both of these results indicate less double-bond character for the urea C–N bond than for an amide C–N bond. Thus, it is apparent that the larger values of J for ligand VI than for ligand I does not result from increased C–N double-bond character.

(21) Stewart, W. E.; Siddall, T. H. *Chem. Rev.* **1970**, *70*, 517–551.
(22) Stilbs, P. *Acta Chem. Scand.* **1971**, *25*, 2635–2642.
(23) Hobson, R. F.; Reeves, L. W.; Shaw, K. N. *J. Phys. Chem.* **1973**, *77*, 1228–1232.
(24) Martin, G. J.; Gouesnard, J. P.; Dore, J.; Rabiller, C.; Martin, M. L. *J. Am. Chem. Soc.* **1977**, *99*, 1381–1384.
(25) Sibi, M. P.; Lichter, R. L. *J. Org. Chem.* **1979**, *44*, 3017–3022.

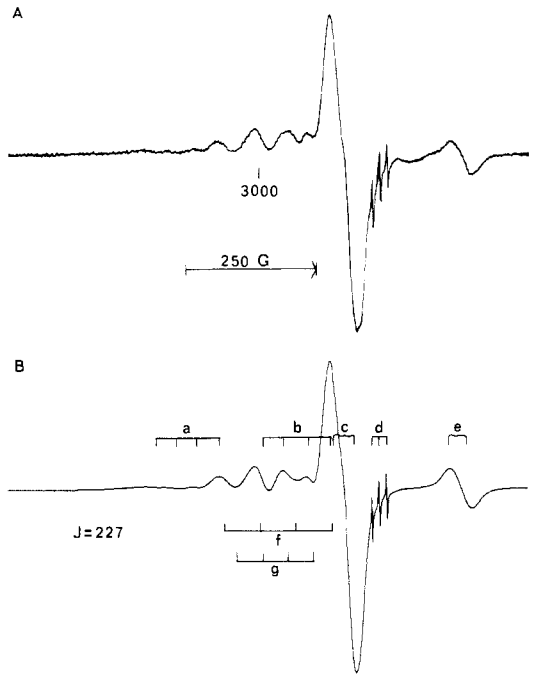

Figure 3. X-Band (9.107 GHz) EPR spectrum of $Cu(hfac)_2$·VI in CH_2Cl_2 solution at room temperature: (A) 1000-G scan obtained with 2-mW power and 1.6-G modulation amplitude; (B) computer-simulated spectra calculated with J = 227 G. The lines in the spectra are assigned to the following: a, copper outer lines; b, copper inner lines; c, range for nitroxyl inner lines; d, free nitroxyl e, range for nitroxyl outer lines; f, free $Cu(hfac)_2$; g, dimer.

A neutron diffraction study of urea showed that the molecule, including the hydrogens, was planar.[26] X-ray crystallographic studies of monosubstituted ureas[27,28] and N,N'-disubstituted ureas[29-31] have shown that the urea linkage is planar and has a trans,trans conformation (XI). NMR,[31]

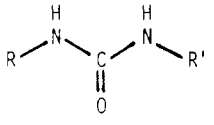

XI

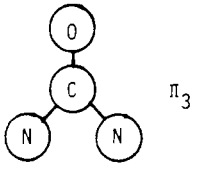

XII

IR,[32,33] and dielectric constant[22] measurements indicate that conformation XI is retained in solution. CNDO calculations have been performed for urea with the assumption of a planar geometry and are in good agreement with photoelectron spectra.[34] These calculations show that C–N double-bond character is due to the π_3 MO, XII, which has approximately equal, in-phase contributions from the π-bonding p orbitals on the two nitrogens, carbon, and oxygen. In both this orbital and its C–N antibonding counterpart, the contributions from the nitrogen lone pairs are in phase. Since the N–N distance is only slightly greater than the C–N distance, it seems plausible that there could be significant electron delocalization via interaction between the two nitrogen lone pairs. Thus, the increase in J for complexes of VI relative to that for I in spite of the extension of the bond pathway by one more atom can be viewed as the result of significant N–N interaction in addition to the N–C–N delocalization pathway in the urea complexes.

Effect of an Additional CH_2 Group on the Value of J. Comparison of the values of J for the 4-substituted urea ligands VI and VII indicates that the additional CH_2 group reduces J by about a factor of 100 for the vanadyl complex and by at least a factor of 100 for the copper complexes. Comparison of the 4-substituted amide ligands I, III, and V indicates that the first CH_2 reduces J by factors of about 20 and 10 for copper and vanadyl, respectively, and the second CH_2 group reduces the value of J by at least another factor of 5–10. For the 3-substituted amides II and IV, the additional CH_2 group reduces the value of J by factors of about 4 and 7 for vanadyl and copper, respectively. Thus, for the amide ligands the impact of a CH_2 group decreases in the order vanadyl complex of a 4-substituted pyridine > copper complex of a 4-substituted ligand ≈ copper complex of a 3-substituted ligand > vanadyl complex of a 3-substituted ligand.

Previous studies of these types of complexes indicate delocalization of the metal unpaired electron involves the pyridine π^* LUMO in the vanadyl complexes and metal–ligand σ bonding in the copper complexes, although significant σ–π mixing occurs in both cases.[5] The pyridine π^* LUMO has a much larger contribution at the 4-position than at the 3-position of the ring. On the basis of these results, we would expect the unpaired spin density in the vanadyl complexes to be greater at the 4-position than at the 3-position and expect the unpaired π-electron spin density at the 4-position to be greater for the vanadyl complexes than for the copper complexes. As discussed above, the impact of a CH_2 group is greater for the vanadyl complexes of the 4-substituted pyridine ligand than for a 3-substituted ligand, and for the 4-substituted pyridine ligands, it is greater for the vanadyl complexes than for the copper complexes. It therefore appears that the impact of the CH_2 group correlates with the magnitude of the π contribution to the spin delocalization. The largest impact of the CH_2 group was observed for the urea ligand VII, which suggests that π delocalization is particularly important for this ligand, consistent with the proposal above that interaction between the nitrogen lone pairs makes a significant contribution to the delocalization pathway.

Acknowledgment. This work was supported in part by NIH Grant GM21156.

Registry No. III, 81194-35-6; IV, 81194-36-7; V, 81194-37-8; VI, 81194-38-9; VII, 81194-39-0; $VO(ttac)_2$·III, 81205-93-8; $VO(hfac)_2$·III, 81205-94-9; $Cu(hfac)_2$·III, 81205-95-0; $VO(tfac)_2$·IV, 81205-96-1; $VO(hfac)_2$·IV, 81205-97-2; $Cu(hfac)_2$·IV, 81205-98-3; $VO(tfac)_2$·V, 81205-99-4; $VO(hfac)_2$·V, 81206-00-0; $Cu(hfac)_2$·V, 81206-01-1; $VO(tfac)_2$·VI, 81206-02-2; $VO(hfac)_2$·VI, 81218-91-9; $Cu(hfac)_2$·VI, 81218-92-0; $VO(tfac)_2$·VII, 81206-03-3; $VO(hfac)_2$·VII, 81218-93-1; $Cu(hfac)_2$·VII, 81206-04-4; $VO(hfac)_2$, 15819-88-2; $Cu(hfac)_2$, 14781-45-4; $Cu_2(hfac)_4$·VI, 81276-60-0; 3-carboxy-2,2,5,5-tetramethylpyrrolin-3-yl-1-oxy acid chloride, 13810-21-4; 3-isocyanato-2,2,5,5-tetramethylpyrrolin-3-yl-1-oxy, 68212-42-0; 4-(aminomethyl)pyridine, 3731-53-1; 3-(aminomethyl)pyridine, 3731-52-0; 4-(aminoethyl)pyridine, 13258-63-4; 4-aminopyridine, 504-24-5.

(26) Worsham, J. E.; Levy, H. A.; Patterson, S. W. *Acta Crystallogr.* **1957**, *10*, 319–323.
(27) Huiszoon, C.; Tiemessen, G. W. M. *Acta Crystallogr., Sect. B* **1976**, *B32*, 1604–1606.
(28) Kashino, S.; Haisa, M. *Acta Crystallogr., Sect. B* **1977**, *B33*, 855–860.
(29) Mootz, D. *Acta Crystallogr.* **1965**, *19*, 726–734.
(30) Kobelt, V. D.; Paulus, E. F. *Acta Crystallogr., Sect. B* **1972**, *B28*, 3452–3457.
(31) Tel, R. M.; Engberts, J. B. F. N. *J. Chem. Soc., Perkin Trans. 2*, **1976**, 483–488.
(32) Mido, Y. *Bull. Chem. Soc. Jpn.* **1974**, *47*, 1833–1837.
(33) Mido, Y. *Spectrochim. Acta, Part A* **1976**, *32A*, 1105–1112.
(34) Dougherty, D.; Wittel, K.; Meeks, J.; McGlynn, S. P. *J. Am. Chem. Soc.* **1976**, *98*, 3815–3820.